(12) INTERNATIONAL APPLICATION PUBLISHED UNDER THE PATENT COOPERATION TREATY (PCT)

(19) World Intellectual Property Organization
International Bureau

(43) International Publication Date
20 October 2016 (20.10.2016)

WIPO | PCT

(10) International Publication Number
WO 2016/168517 A1

(51) International Patent Classification:
G01B 7/26 (2006.01) *G01R 33/32* (2006.01)
G01B 7/02 (2006.01) *G01R 33/422* (2006.01)
G01B 7/28 (2006.01) *G06F 1/00* (2006.01)
G01R 33/12 (2006.01)

(21) International Application Number:
PCT/US2016/027624

(22) International Filing Date:
14 April 2016 (14.04.2016)

(25) Filing Language: English

(26) Publication Language: English

(30) Priority Data:
62/149,159 17 April 2015 (17.04.2015) US

(71) Applicant: **NEW YORK UNIVERSITY** [US/US]; 70 Washington Square South, New York, New York 10012 (US).

(72) Inventors: **JERSCHOW, Alexej**; 4 Washington Square Village 5R, New York, New York 10012 (US). **ILOTT, Andrew J.**; c/o New York University, 70 Washington Square South, New York, New York 10012 (US).

(74) Agents: **MARTIN, Matthew E.** et al.; Foley & Lardner LLP, 3000 K Street N.W., Suite 600, Washington, District of Columbia 20007 (US).

(81) **Designated States** *(unless otherwise indicated, for every kind of national protection available)*: AE, AG, AL, AM, AO, AT, AU, AZ, BA, BB, BG, BH, BN, BR, BW, BY, BZ, CA, CH, CL, CN, CO, CR, CU, CZ, DE, DK, DM, DO, DZ, EC, EE, EG, ES, FI, GB, GD, GE, GH, GM, GT, HN, HR, HU, ID, IL, IN, IR, IS, JP, KE, KG, KN, KP, KR, KZ, LA, LC, LK, LR, LS, LU, LY, MA, MD, ME, MG, MK, MN, MW, MX, MY, MZ, NA, NG, NI, NO, NZ, OM, PA, PE, PG, PH, PL, PT, QA, RO, RS, RU, RW, SA, SC, SD, SE, SG, SK, SL, SM, ST, SV, SY, TH, TJ, TM, TN, TR, TT, TZ, UA, UG, US, UZ, VC, VN, ZA, ZM, ZW.

(84) **Designated States** *(unless otherwise indicated, for every kind of regional protection available)*: ARIPO (BW, GH, GM, KE, LR, LS, MW, MZ, NA, RW, SD, SL, ST, SZ, TZ, UG, ZM, ZW), Eurasian (AM, AZ, BY, KG, KZ, RU, TJ, TM), European (AL, AT, BE, BG, CH, CY, CZ, DE, DK, EE, ES, FI, FR, GB, GR, HR, HU, IE, IS, IT, LT, LU, LV, MC, MK, MT, NL, NO, PL, PT, RO, RS, SE, SI, SK, SM, TR), OAPI (BF, BJ, CF, CG, CI, CM, GA, GN, GQ, GW, KM, ML, MR, NE, SN, TD, TG).

Declarations under Rule 4.17:

— *as to applicant's entitlement to apply for and be granted a patent (Rule 4.17(ii))*

Published:

— *with international search report (Art. 21(3))*

[Continued on next page]

(54) Title: SYSTEMS AND METHODS FOR SUPER-RESOLUTION SURFACE-LAYER MICROSCOPY USING MAGNETIC RESONANCE

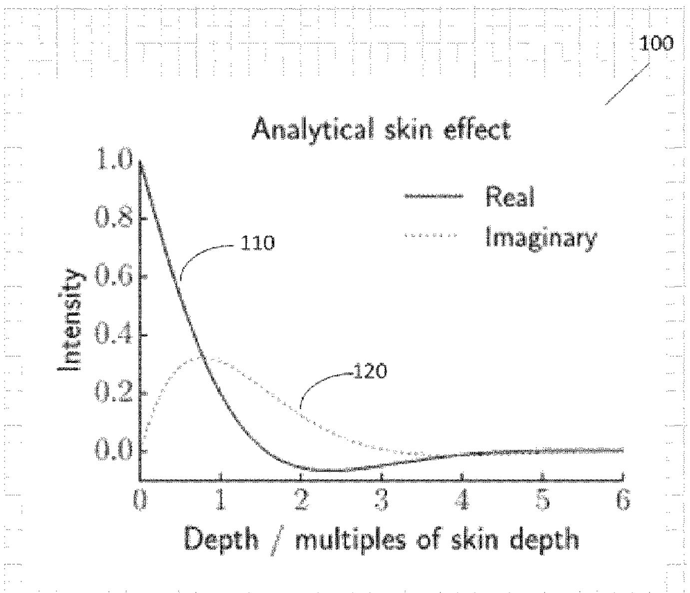

Fig. 1

(57) Abstract: Systems and methods for using and exploiting the effect of electromagnetic field distortions (skin effect) induced by conductive or semi-conductive materials or phases of matter in order to excite and detect spins at specific depths within such matter, with a selectivity of approximately 0.25δ. This technique allows the acquisition of a depth profile of a conductor with a resolution far exceeding that of any MRI experiment and without the use of external magnetic field gradients, thus it is appropriately called a super-resolution methodology. Furthermore, the sequence can be combined with other MR sequences or imaging techniques to take depth-dependent measurements. At the heart of these super-resolution techniques lie not just the principle of reciprocity as formulated within the context of magnetic resonance, but also the specific dependence of the signal phases in response to propagation within conductive media.

WO 2016/168517 A1

— *before the expiration of the time limit for amending the claims and to be republished in the event of receipt of amendments (Rule 48.2(h))*

SYSTEMS AND METHODS FOR SUPER-RESOLUTION SURFACE-LAYER MICROSCOPY USING MAGNETIC RESONANCE

STATEMENT OF GOVERNMENT INTEREST

[0001] The United States Government has rights in the invention described herein pursuant to the award CHE-1412064 from the US National Science Foundation.

CROSS-REFERENCE TO RELATED PATENT APPLICATIONS

[0002] This application claims priority from Provisional Application US Application 62/149,159, filed 4/17/2015, incorporated herein by reference in its entirety.

FIELD OF THE INVENTION

[0003] The present invention generally relates super resolution microscopy. In particular, the present invention relates to super-resolution microscopy using magnetic resonance.

BACKGROUND OF THE INVENTION

[0004] Resolution of items beyond the limits of optical microscopes due to the diffraction of light has become increasingly important. However, such "super resolution" microscopy techniques have proven lacking in application to certain subjects.

[0005] However, techniques have been developed for determining properties for a subject, for example Magnetic Resonance is used for conductive regions. In magnetic resonance imaging, localization is performed with the help of magnetic field gradients. Electromagnetic radiation decays exponentially when it enters a conducting region with a characteristic length, called the skin depth,

$$\delta = \sqrt{\frac{1}{\pi\mu\nu\sigma}} \qquad \text{(Equation 1)}$$

where ν is the frequency of the field, μ the permeability of the conductor and σ its conductivity. This effect has profound implications for the sensitivity of magnetic resonance (MR) techniques, which rely on radio frequency (rf) fields to excite and detect precessing spins from within conducting regions.

[0006] A key feature Equation 1 above is the dependence on $\nu^{-1/2}$ which means that at higher frequencies (corresponding to experiments performed at higher magnetic fields) δ is reduced. For example, $\delta = 12.3\,\mu\text{m}$ for nuclear spins of Lithium-7 (^{7}Li) in metallic lithium at a magnetic field of a 9.4 T (larmor frequency, $\nu_\text{n} = 155$ MHz) while Lithium-6 (^{6}Li) nuclei in the same sample will have a larger effective skin depth, $\delta = 20.0\,\mu\text{m}$ because of the lower gyromagnetic ratio of this isotope and therefore lower larmor frequency ($\nu_\text{n} = 59$ MHz). For a corresponding electron spin transition, GHz frequencies would be relevant, and the skin depth would be in the range $\delta \approx 1\mu\text{m}$.

SUMMARY OF THE INVENTION

[0007] In one implementation, the disclosure describes a method of probing the layers above, at, and below the surface of a conducting region. The nuclear or electronic spins present in a conductive region are excited by a frequency. A frequency is then detected from the conducting region. Using the conductivity of the conducting region, the frequency used to excite the nuclear or electronic spins, and the frequency that is detected, the length scales are determined. The depth profile of the conducting region can then be obtained.

[0008] In another implementation, the disclosure describes a method of applying a pulse sequence to a conducting region. The pulse sequence is comprised of several rf pulses and delays and results in impregnating the conducting region with a pattern of z-magnetization. A detector can than read out the pattern of z-magnetization.

[0009] It would be useful to achieve resolution along one or more imaging dimension exceeding typical resolution limits of even magnetic resonance imaging (MRI) machines. The concepts discussed can be extended to other microscopy, including optical microscopy.

BRIEF DESCRIPTION OF THE FIGURES

[0010] The foregoing and other objects, aspects, features, and advantages of the disclosure will become more apparent and better understood by referring to the following description taken in conjunction with the accompanying drawings, in which:

[0011] Fig. 1 illustrates the form of the analytical skin depth equation in the rotating frame. The field at the surface is assumed to be $\boldsymbol{B}_0 = 1 + 0i$.

[0012] Fig. 2 illustrates the changing flip angle as a function of the depth in a conductor.

[0013] Fig. 3 illustrates a graph of an experimental ^{7}Li nuclear magnetic resonance nutation curve for a lithium metal strip plotted alongside a numerical solution and a solution that solves the Bloch equations to include relaxation during the pulse

[0014] Fig. 4 illustrates a pulse sequence designed to selectively excite the magnetization at one value of r while saturating the magnetization at other depths.

[0015] Fig. 5 illustrates plots for the solution of the Bloch equations for the π pulse chain in the saturation pulse sequence with $N = 6$ and variable k for $r = 0, 0.5\delta, \delta$.

[0016] Fig. 6 illustrates simulation results of the sequence shown in Fig. 4 for different values of k, with $N = 16, \Delta = 800\ \mu s$, $T_1 = 170$ ms and $T_2 = 500$ µs.

[0017] Fig. 7 illustrates a demonstration of the sequence results for samples of different shape.

[0018] Fig. 8 illustrates experimental results obtained by varying k (by changing the pulse duration, τ, with $\alpha(r = 0) = \pi$ corresponding to a $108\ \mu s$ pulse as calibrated on LiCl(aq)) in the pulse sequence in Fig. 4 with $N = 16$ and $\Delta = 800\ \mu s$.

[0019] Fig. 9 illustrates one embodiment of a computer system for implementing an embodiment of the methods described herein.

[0020] Figs. 10A-C illustrate one embodiment of an MRI setup: Fig. 10A illustrates the rf coil or resonator covers the full sample volume, and surface layers of the conducting region are probed by the pulse sequence. In addition morphological details are probed above the surface via the susceptibility differences between the materials. Fig. 10B illustrates the coil or resonator can be situated above the surface and scan the surface of the material in a setup similar to atomic force microscopy or magnetic resonance force microscopy. The local surface layers are probed by the pulse sequences described. Fig. 10C illustrates morphological details are obtained by (a) probing the surface penetration of the electromagnetic fields and using the pulse sequences (b) probing morphology is also performed by visualizing the changes above the surface.

[0021] Figs. 11 A-F illustrate a demonstration of frequency changes around a conducting microstructure region, calculated via finite element methods. The histogram shows the frequency distributions.

[0022] Fig. 12A-C illustrate *In situ* ^{1}H 3D FLASH imaging results from the electrochemical cell charged at 160 μA. Fig. 12A shows 2D slices from four time points, Fig. 12B shows segmented images of the results from Fig. 12A where $\boldsymbol{I}_{\mathbf{threshold}} = \mathbf{0.2}\boldsymbol{I}_{\mathbf{max}}$, Fig. 12C shows 3D segmented images of the same time points with an additional Gaussian filter applied to smoothen the visualization.

[0023] Fig. 13A-C shows the geometry of a commercial coin cell, but with the side casing made of non-conducting material.

[0024] In the following detailed description, reference is made to the accompanying drawings, which form a part hereof. In the drawings, similar symbols typically identify similar components, unless context dictates otherwise. The illustrative embodiments described in the detailed description, drawings, and claims are not meant to be limiting. Other embodiments may be utilized, and other changes may be made, without departing from the spirit or scope of the subject matter presented here. It will be readily understood that the aspects of the present disclosure, as generally described herein, and illustrated in the figures, can be arranged, substituted, combined, and designed in a wide variety of different configurations, all of which are explicitly contemplated and made part of this disclosure.

DETAILED DESCRIPTION OF THE INVENTION

[0025] Magnetic Resonance ("MR") studies of metals have emerged, largely due to applications in battery systems, where insight into the processes occurring on the metal surface is sought. Described herein are systems and methods utilizing the skin effect to provide an advantage by ensuring that all the detected signal originates from the area of interest: the surface.

[0026] One implementation described in the present disclosure relates to a methodology by which the skin effect can be exploited in order to excite and detect spins at specific depths within a conductor, with a selectivity of approximately 0.25δ. This technique allows the acquisition of a depth profile of a conductor with a resolution far exceeding that of any MRI experiment and without the use of external magnetic field gradients, thus it is appropriately called a super-resolution methodology. Furthermore, the sequence can be combined with other MR sequences or imaging techniques to take depth-dependent measurements.

[0027] At the heart of these super-resolution techniques lie not just the principle of reciprocity as formulated within the context of magnetic resonance, but also the specific dependence of the signal phases in response to propagation within conductive media.

Signal Detection in Magnetic Resonance: The Principle of Reciprocity

[0028] The orthogonal components of the applied radiofrequency field, $\boldsymbol{B}_{1\mathrm{x}}$ and $\boldsymbol{B}_{1\mathrm{y}}$ (where the bold notation signifies a complex quantity), can be used to define the rf field in the rotating frame of the nuclear spins,

$$\widetilde{\boldsymbol{B}}_1^+ = \tfrac{1}{2}\left(\boldsymbol{B}_{1\mathrm{x}} + i\boldsymbol{B}_{1\mathrm{y}}\right), \qquad \text{(Equation 2)}$$

$$\widetilde{\boldsymbol{B}}_1^- = \tfrac{1}{2}\left(\boldsymbol{B}_{1\mathrm{x}} - i\boldsymbol{B}_{1\mathrm{y}}\right)^*, \qquad \text{(Equation 3)}$$

where $\widetilde{\boldsymbol{B}}_1^+$ is the field in the positively rotating frame, and $\widetilde{\boldsymbol{B}}_1^-$ is the field in the negatively rotating frame.

[0029] Given an equilibrium magnetization, M_0, and an rf field as indicated by the equations above for a duration τ, the complex transverse magnetization in the positive rotating frame becomes

$$\widetilde{\boldsymbol{M}}^+ = M_0 \sin\left(\gamma\tau|\widetilde{\boldsymbol{B}}_1^+|\right)\frac{-i\widetilde{\boldsymbol{B}}_1^+}{|\boldsymbol{B}_1^+|}, \qquad \text{(Equation 4)}$$

where γ is the gyromagnetic ratio, and $\widetilde{\boldsymbol{M}}^+$ represents the *x* and *y* components of the magnetization in the rotating frame, $\widetilde{\boldsymbol{M}}^+ = \widetilde{M}_{\mathrm{x}} + i\widetilde{M}_{\mathrm{y}}$.

[0030] The detected signal arises from the induced magnetic flux at the detection coil by the precessing spin magnetization. For reciprocity to hold, the strength of this signal has an added dependence on the intrinsic sensitivity of the coil, which is represented by the field in the negatively rotating frame produced by a unit current in the coil, $\widehat{\boldsymbol{B}}_1^{-*}$. The voltage induced in the coil is,

$$\boldsymbol{\epsilon} = 2\omega\widetilde{\boldsymbol{M}}^+\widehat{\boldsymbol{B}}_1^{-*}. \qquad \text{(Equation 5)}$$

This quantity multiplied by $e^{i\omega t}$ (and e^{t/T_2^*}) gives the form of the acquired signal in the laboratory frame as a function of time.

Skin effect in conductors

[0031] When incident on a conductor, the magnitude of the rf field is attenuated while the phase of the wave is also modified at different depths,

$$\boldsymbol{B} = \boldsymbol{B}_0 e^{-\beta \bar{\mathrm{n}} \cdot \bar{\mathrm{r}}} e^{i\alpha \bar{\mathrm{n}} \cdot \bar{\mathrm{r}} - i\omega t}, \quad \text{(Equation 6)}$$

where α and β are the real and imaginary parts of the wave vector, $\boldsymbol{k} = \alpha + i\beta$, whose full form is given by,[1]

$$\left.\begin{matrix}\alpha\\ \beta\end{matrix}\right\} = \sqrt{\mu\varepsilon}\frac{\omega}{c}\left[\frac{1}{2}\sqrt{1+\left(\frac{2\sigma}{\nu\varepsilon}\right)^2} \pm \frac{1}{2}\right]^{1/2}, \quad \text{(Equation 7)}$$

where ε is the dielectric constant of the conductor and c is the speed of light in a vacuum. For a good conductor $\left(\frac{2\sigma}{\nu\varepsilon}\right) \gg 1$ and $\alpha \approx \beta$ $(= 1/\delta$, the inverse of the skin depth constant as defined by Equation 1), resulting in the same depth-dependence for both the phase and amplitude of the wave. For reference, for lithium metal, $\sigma = 1.08 \text{ x } 10^7$, $\varepsilon = \varepsilon_r \varepsilon_0 = (1+\chi)\varepsilon_0 \approx (1 + 2 \text{ x } 10^{-5}) \text{ x } 8.9 \text{ x } 10^{-12}$, which comfortably places it as a good conductor at typical nuclear magnetic resonance (NMR) or electron spin resonance (ESR) frequencies.

[0032] When $\bar{n}$ and $\bar{r}$ are parallel for wave propagation into the surface, Equation 6 becomes

$$\boldsymbol{B} = \boldsymbol{B}_0 e^{-\beta r} e^{i(\beta r - \omega t)}. \quad \text{(Equation 8)}$$

While the amplitude of the field is attenuated according to $e^{-\beta r}$, the phase at a given depth is proportional to βr.

[0033] If observing only the signal from the conductor, then Equation 8 can be considered as describing the $\boldsymbol{B}_1$ field, and the x, y subscripts can be dropped by ensuring that $\boldsymbol{B}_1$ is aligned with the surface of the conductor. The expressions for the positively and negatively rotating frame become

$$\widetilde{\boldsymbol{B}}_1^+(r) = \boldsymbol{B}_0 e^{-\beta r} e^{i\beta r}, \quad \text{(Equation 9)}$$

$$\widetilde{\boldsymbol{B}}_1^-(r) = \left(\boldsymbol{B}_0 e^{-\beta r} e^{i\beta r}\right)^*, \quad \text{(Equation 10)}$$

$$|\widetilde{\boldsymbol{B}}_1^+(r)| = |\boldsymbol{B}_0| e^{-\beta r}, \quad \text{(Equation 11)}$$

where, for convenience, the factor of 1/2 in Equations 2 and 3 has been absorbed by the $\boldsymbol{B}_0$ term.

[0034] The form of $\widetilde{\boldsymbol{B}}_1^+(r)$ is shown in Fig. 1, which shows the form of the analytical skin depth equation in the rotating frame 100. The field at the surface is assumed to be $\boldsymbol{B}_0 = 1 + 0i$. The real component 110 is graphed using a solid line. The imaginary component 120 is graphed using a dashed line.

[0035] Substituting the expression for $\widetilde{\boldsymbol{B}}_1^+(r)$ into Equation 4 gives the flipped magnetization at each depth,

$$\widetilde{\boldsymbol{M}}^+(r) = -i \frac{M_0 \boldsymbol{B}_0}{|\boldsymbol{B}_0|} e^{-i\beta r} \sin\left(\gamma\tau |\boldsymbol{B}_0| e^{-\beta r}\right), \quad \text{Equation 12}$$

and the voltage induced in the detection coil is given by the integral of the contributions from each depth, scaled by the detection signal strength which is also depth dependent:

$$\epsilon = -2i\omega \frac{\boldsymbol{B}_0^2}{|\boldsymbol{B}_0|} M_0 \int_{r=0}^{\infty} e^{2i\beta r} e^{-\beta r} \sin\left(\gamma\tau |\boldsymbol{B}_0| e^{-\beta r}\right) dr. \quad \text{Equation 13}$$

The time dependence would be obtained by multiplying by $e^{i\omega t}$ (and e^{t/T_2^*}) as before.

[0036] There are some key aspects of this expression that have many implications for the MR signal acquired from conductors. Firstly, the $e^{-\beta r}$ term inside the integral scales the signal acquired at higher r (deeper into the conductor). Similarly, the $e^{2i\beta r}$ term ensures that the relative phase of the acquired signal is proportional to the depth, this term governs the extent of constructive or deconstructive interference between the signals from different depths during a given excitation. Finally, the $e^{-\beta r}$ term inside the sine function governing the nutation of the magnetization in the rotating frame ensures that spins at each depth are flipped by a different angle, as we discuss below.

Nutation: Simulation and Experiment

[0037] The effects implied by Equation 13 have a direct impact on signal quantification, but a much more sensitive measure of the full form of the equation and therefore a method by which to validate reciprocity, is a nutation experiment in which the signal is measured as a function of the excitation pulse duration, τ.

[0038] In the vector model, the flip angle, α, is defined as the angle through which the bulk magnetization vector is rotated by the rf field. In a conductor, this equates to the quantity inside the sine term in Equation 12, and it is depth dependent,

$$\alpha(r) = \gamma\tau|\boldsymbol{B}_0|e^{-\beta r}, \quad \text{Equation 14}$$

so that for a given rf field strength, $|\boldsymbol{B}_0|$, and duration, τ, magnetization at each depth in the conductor will be excited by a different flip angle. This effect is illustrated in Fig. 2. The depth-dependence of the phase will not impact the flip angle, but will change the relative size of the x and y components of $\widetilde{\boldsymbol{M}}^+$ at each depth. The acquired NMR signal is a sum over the signals from every depth and the phase of the excited magnetization is crucial in determining the overall sum. Only by comparing the relative signal intensities at different flip angles can the effect of the phase be judged. Described herein is a nutation experiment in which signal is acquired for multiple values of τ.

[0039] Fig. 2 shows an illustration of the changing flip angle as a function of the depth in a conductor 200. The position corresponding to a π pulse is indicated for two cases with differing flip angles at the surface. The line 210 corresponding to a starting angle of 1.3π is shown. The line 220 corresponding to a starting angle of 2.0π is similarly shown.

[0040] An experimental ^{7}Li NMR nutation curve 330 performed on a rectangular piece of natural abundance lithium metal (approximately 10 x 20 x 0.5 mm) is shown in Fig. 3 along with numerical simulations based on Equations 6-14. Fig. 3 shows a Bloch simulation plot 310 of a solution that solves the Bloch equations to include relaxation during the pulse. The flip angle defined by the x axis is calibrated to LiCl(aq) in the experimental curve and to $\boldsymbol{B}_0$ in the calculated curves. The numerical simulation of Equation 13 plot 320 is also shown as well as the experimental ^{7}Li NMR nutation curve 330 for a lithium metal strip. Solid and dotted lines for all plots represent the real and imaginary components of the nutation curves, with the solid lines representing the real components and the dotted lines representing the imaginary components.

[0041] The appearance of these curves 300 is very distinctive and contrast sharply with that expected for a liquid sample, where a damped, sinusoidal pattern would be observed (Equation 4). It is seen that there is excellent agreement between the experimental curve and the calculated ones, particularly at lower flip angles $< 3\pi$ where the forms of both the real and imaginary signals are reproduced, as well as their relative magnitude. A slight offset is apparent in the position of the first minimum in the calculated curves that can be ascribed to slight deviations in flip angle calibration. Although, in the experiment LiCl(aq) is used for pulse calibration, it is expected that the field in close proximity to the metal surface is attenuated. A second discrepancy can be found at larger flip angles, where the experimental curve appears to be somewhat attenuated relative to the calculated curves. A simulation including relaxation effects during the pulse (top line) agrees better in these regions, but not completely, implying that relaxation effects cannot be the sole reason for this discrepancy. The remaining discrepancy could be explained by inhomogeneities in the rf field at the surface of the conductor which would mean that the result represents a superposition of nutation curves for a range of effective $\boldsymbol{B}_0$ values, damping the oscillations in the curve at higher flip angles.

[0042] It is worth considering how the different terms in Equation 13 impact the nutation curve. Without the $e^{2i\beta r}$ term (which would be cancelled out if the complex conjugate of $\widehat{\boldsymbol{B}}_1^{-*}$ were not taken in Equation 13) there would be no depth-dependent phase and the real component of the induced voltage would always be zero (ignoring any off-resonance effects). A similarly incorrect nutation curve would also be obtained if the $e^{-\beta r}$ term were neglected by not taking into account the detection field; in this case the signal from within the metal would contribute more strongly, particularly when the flip angle near the surface is a multiple of π.

[0043] The sensitivity of the nutation curve to the formulation of the equation for the detected signal provides a practical proof of the theory of reciprocity. Moreover, this effect also confirms that the mathematical basis for understanding skin effects is accurate. This formalism opens up the possibility of designing more advanced pulse sequences to exploit the depth dependence of the rf to selectively probe different regions of the conductor.

Pulse Sequence: Depth Selective Saturation and Excitation in Conductors

[0044] Fig. 4 shows a pulse sequence 400 that, by exploiting the depth dependence of the flip angle (Fig. 2), can be used to selectively excite the magnetization at only one depth inside the conductor, while saturating the magnetization at other depths. The sequence consists of a chain of N $k\pi$ pulses separated by time delays, Δ 410, followed by a readout $k\pi/2$ pulse 420. The value of k is chosen to adjust $\alpha(r = 0)$, but only the selected magnetization at depths where $\alpha(r_{\text{sel}}) = \pi$ is preserved after the initial pulse chain, as described below.

[0045] Fig. 5 illustrates the solution of the Bloch equations for the π pulse chain in the saturation pulse sequence with $N = 6$ and variable k for $r = 0, 0.5\delta, \delta$. $|M_{\text{xy}}|$ (dotted line) and M_{z} (solid line) are plotted. The black regions indicate evolution under an rf pulse. Relaxation during the pulses is neglected, but would not produce sizable deviation.

[0046] Fig. 5 shows the effect that the π pulses have on the magnetization at different positions in the conductor. When $k = 1$ (Fig. 5, panel (b)) the magnetization at the surface ($r = 0$) is initially inverted from its equilibrium state at $M_{\text{z}} = M_0$, $M_{\text{xy}} = 0$ to $M_{\text{z}} = -M_0$, $M_{\text{xy}} = 0$ and is in general stored along the z axis following each pulse. Therefore, during the evolution periods the magnetization is affected by the T_1 relaxation mechanisms only because $M_{\text{xy}} = 0$, and when $T_1 \gg T_2$, as is the case for ^{7}Li metal, to a good approximation, the magnetization in this region is preserved throughout the π pulse chain. Due to the skin effect, regions away from the surface experience a damped $\widetilde{\boldsymbol{B}}_1^+$ field and so experience a reduced flip angle $< \pi$ (Fig. 2). The simulations for sites at $r = 0.5\delta, \delta$ in Fig. 5, panel (b) illustrate the effect that this has; the magnetization is not stored along z, but has some xy component that quickly relaxes during the evolution periods. After multiple cycles of this process both the xy and z components of the magnetization are saturated, leaving signal from $r = 0$ only. Fig. 5 (panels (a) and (c)) show that by changing k and therefore the flip angle at $r = 0$, different positions in the metal are selectively excited or saturated. More specifically, for a given value of k only the signal at a selected depth where $\alpha(r_{\text{sel}}) = \pi$ is preserved. That is, $\alpha(r_{\text{sel}}) = \pi = k\pi e^{-\beta r_{\text{sel}}}$, from Eq. 14, giving

$$r_{\text{sel}} = \delta \ln k, \qquad \text{Equation 15}$$

where $\delta = 1/\beta$.

[0047] Fig. 6 illustrates simulation results 600 of the sequence shown in Fig. 4 for different values of k, with $N = 16$, $\Delta = 800\,\mu s$, $T_1 = 170$ ms and $T_2 = 500$ µs. Fig. 6, panel (a) shows the absolute value of the detected signal at each depth. Fig. 6, panel (b) shows the summed signal over all the simulated depths

[0048] As shown in Fig. 6, the full simulation for different k values at different depths (Fig. 6, panel (a)) demonstrates clearly that the dominant signal acquired for each k does occur around $\delta \ln k$ with a selectivity of ca. $\delta/4$ (3 µm for ^7Li at 155 MHz). At $k = 2$ there is an extra region of signal intensity at $r = 0$ because the flip angle at the surface is close to 2π, so that the magnetization there is stored along $+z$ during the saturation pulse chain and is preserved. However, the acquired signal intensity still remains low in this region because $\alpha_{\text{readout}}(r = 0) = \pi$ and so the magnetization remains along $-z$ and is not observed, although regions close to $r = 0$ where α_{readout} deviates slightly from π do contribute some observable xy magnetization. This case will occur at all even values of k. A similar argument can also be followed for odd values of $k > 1$, however in these regions the readout pulse is a multiple of $\pi/2$ so they contribute a large signal intensity to the overall sum. These effects are observed in Figs. 6(a) and 6(b) where perturbations in the curve 610 are noticeable close to $k = 2$ and 3. Their overall impact could be minimized by increased N or by implementing a phase cycle for the acquisition. Restricting experiments to $k < 2$ would ensure that the region of interest is unambiguously defined and would still provide fine resolution of the surface sites in the conductor.

[0049] Fig. 7 illustrates the demonstration of the sequence results for samples of different shapes. In Fig. 7, panel (a) shows the shape function assuming uniform density. Fig. 7, panel (b) shows simulated 2D profile for each shape showing signal intensity as a function of k and r. Fig. 7, panel (c) shows 1D profiles that could be measured experimentally by varying k. Fig. 7, panel (d) shows the transform of the simulated results from panel (c) to recover the underlying shape functions.

[0050] Until now the disclosure has focused on a sample with a uniform number of spins at each depth, corresponding to a planar surface with a thickness much greater than δ. To consider conducting samples consisting of different shaped structures, the shape function, $S(r)$, is defined that represents the number of nuclear spins at each depth in the sample. Examples of $S(r)$ for the planar surface explored previously and for cylinders and spheres with radii $\delta/2$ are given in Fig. 7, panel (a), assuming a constant spin density over the sample volume in each case. The shape function directly scales the detected signal at each depth and therefore the signal amplitude detected in an experiment using a given k (substituting Equation 15 into Equation 13, assuming $\alpha_{\text{readout}}(r_{\text{sel}}) = \pi/2$ and taking the magnitude),

$$|\epsilon(k)| = \frac{1}{k} S(r_{\text{sel}}), \quad \text{Equation 16}$$

[0051] The effect is apparent for the shapes explored in Fig. 7, panel (b), where the signal at $r > 0$ for the sphere and cylinder is attenuated relative to the results for the infinite plane. This effect, in turn, makes a significant impact on the measurable profiles in Fig. 7, panel (c). However, Equation 16 demonstrates how the measurements of $|\epsilon(k)|$ can be converted to recover the underlying shape function, by transforming the measured signal by $k|\epsilon(k)|$ and by transforming k to the selected depth, $r = \delta \ln k$. Fig. 7, panel (d) demonstrates the outcome of this process for the simulated results, showing that $S(r)$ is accurately reconstructed in each case, although there is some deviation at $r = 0 (k = 1)$, which can be explained by the finite thickness of the excited region in Fig. 7, panel (b); at $r = 0$ the region covers half the area it does at larger depths, and so the sum contribution to the signal intensity is reduced (in fact it should be exactly half the maximum value at $r = 0$).

[0052] Fig. 8 illustrates the experimental results 820 obtained by varying k (by changing the pulse duration, τ, with $\alpha(r = 0) = \pi$ corresponding to a $108\,\mu s$ pulse as calibrated on LiCl(aq)) in the pulse sequence in Fig. 4 with $N = 16$ and $\Delta = 800\,\mu s$. The intensity of the on-resonance position in the frequency domain spectrum is plotted 800. The simulated curve 810 is taken from the sum over all depths of a simulation employing the same parameters as used experimentally, including the pulse widths.

[0053] Experimental results 820 using the pulse sequence from Fig. 4 are shown in Fig. 8 with the corresponding simulation results 810. A similar behavior is observed in both simulation and experiment, with a maximum intensity in both the real 830 and imaginary 840 components of the signal at $k = 1$, corresponding to the selection of the slice at the top surface of the ^{7}Li metal. According to Fig. 6, panel (a), this slice can be expected to be $2 - 3\mu$m thick. The decay of the signal at $k > 1$ is slightly different for the simulated 810 and experimental 820 results, which may be due to differences in the relaxation behavior, although the simulations do include relaxation during the pulses and pulse lengths match those used in the experiment. With higher power pulses, relaxation effects would be less important, and so longer chains of π pulses could be used to enhance the saturation without significantly reducing the signal amplitude. It is assumed that the surface of the metal is smooth and chemically pure on the length scales that is being probed. On the other hand it is likely that some surface roughness contributes to the deviations, particularly because ^{7}Li metal is air sensitive (the sample is prepared and sealed in an argon environment).

[0054] Even without understanding the effects at $k > 1$, simply by recording the curve in Fig. 8 and selecting the value of k that gives the maximum signal is sufficient to optimize the sequence to select only surface sites. This approach also circumvents any problems assessing the actual field strength at the surface of the metal or using a reference sample.

[0055] In one embodiment, the method of probing the method of probing the layers above, at, and below the surface of a conducting region comprises exciting nuclear or electronic spins within the conducting region using a first frequency and receiving a second frequency from the conducting region. The length scales are determined by the conductivity of the conducting region and the first frequency and a depth profile is obtained of the conducting region. The conducting region may be composed of various conductive or semi-conductive matter or states of matter including metallic conductors, semi-conductors, plasmas, electrolyte solutions, superconductors, etc. The method may further comprise tuning the length scale by choosing the operating frequency. The first frequency may be the same or substantially the same as the second frequency or the two frequencies may be different frequencies.

[0056] In one implementation of one embodiment where the first and second frequencies are different, the difference may be due to such magnetization transfer effects as cross-polarization, insensitive nuclei enhanced by polarization transfer (INEPT), distortionless enhancement by polarization transfer (DEPT) or other effects and methods known in the art.

[0057] In one implementation of one embodiment the receiving of the second frequency step is done or accomplished using the induced magnetic flux in a detection coil by the precessing spin magnetization.

[0058] In another embodiment the method of probing the layers above, at, and below the surface of a conducting region may also comprise applying a shape function to the signal received from the detection coil, wherein the shape function directly scales the detected signal at each depth.

[0059] In another embodiment, the method of the disclosure may consist of applying a pulse sequence to a conducting region by applying a pulse sequence comprising several rf pulses and delays, wherein the pulse sequence impregnates the conducting region with a certain pattern of z-magnetization and then reading out the pattern of the z-magnetization. The pattern may be the result of the application of repeated pulses which are attenuated and phase-shifted within the conducting region. The pattern may be adjusted within the conducting region by altering delays, pulse flip angles and repeats in the pulse sequence. Alternatively the pattern may be adjusted by the repeat of the pulse sequence with modified rf pulse phases. Alternatively, the pattern may be adjusted through induced changes in conductivity within the layers of the conducting region. Alternatively, the pattern may be adjusted by changes in magnetic resonance relaxation parameters.

[0060] In another embodiment, the method of applying a pulse sequence to a conducting region of may take repeated measurements obtained from the reading out the pattern step to quantify the concentration of electron or nuclear spins within the conducting region.

[0061] In another embodiment, the method of applying a pulse sequence to a conducting region may use the read out pattern of z-magnetization to measure magnetic resonance parameters. Alternatively, the read out pattern may be used to measure diffusion or flow within the conducting region. The measured diffusion along with a depth profile may be used as a spectrometer or in spectroscopy measurements.

[0062] In one embodiment, the method for creating a pulse sequence uses the skin effect in a good conductor which ensures the spatial dependence of the rf field strength and uses flip angle $T_1 > T_2$ because the magnetization from the target depth is stored along the z axis and relaxes via T_1 while the unwanted magnetization relaxes via T_2. The second process may be faster to saturate the unwanted magnetization while preserving that at the target depth. Different sequences are designed for different T_1/T_2 combinations, particularly if they are known for a given sample. Alternately, the embodiment makes a sequence immune to short T_2 using a 2-step phase cycle to give some selectivity but not saturate the magnetization at different depths.

[0063] In another embodiment, the π pulse chain saturates the magnetization at all but a region around the selected depth thus preparing the magnetization prior to the application of a more complex sequence, allowing the depth dependence of other properties to be explored. Then the combination of chemical shift and depth profile can give information on the composition of the surface and interface resulting in spectroscopy.

[0064] In another embodiment, the π pulse chain saturates the magnetization at all but a region around the selected depth thus preparing the magnetization prior to the application of a more complex sequence, allowing the depth dependence of other properties to be explored. Then imaging sequences (short echo time, radial, frequency-encoded sequences in particular) are applied thus revealing the spatial distribution of select depths of the conductor. This may be used to differentiate between regions containing structures of different thickness (i.e. dendrites vs bulk electrode).

[0065] In another embodiment, the π pulse chain saturates the magnetization at all but a region around the selected depth thus preparing the magnetization prior to the application of a more complex sequence, allowing the depth dependence of other properties to be explored. Then cross polarization sequences are applied to measure the distance from the surface sites of a conductor to any NMR active nuclei in close proximity. This may then be used to establish that a species is adsorbed or bound to the surface, and transferred magnetization could be used with standard pulse sequences to get properties of the adsorbed species.

[0066] In another embodiment, the π pulse chain saturates the magnetization at all but a region around the selected depth thus preparing the magnetization prior to the application of a more complex sequence, allowing the depth dependence of other properties to be explored. Then, T_2 measurements may give information on the local dynamics and magnetic interactions

[0067] In another embodiment, the π pulse chain saturates the magnetization at all but a region around the selected depth thus preparing the magnetization prior to the application of a more complex sequence, allowing the depth dependence of other properties to be explored. Then, $T_{1\rho}$ measurements may probe dynamics on kH timescales very relevant to chemical reactions and other processes occurring on the surface.

[0068] In another embodiment, the systems and methods of the disclosure may have relevance to any NMR-active nucleus inside a conductor (not restricted to metals), lithium and sodium battery systems, and/or superconductors.

[0069] In another embodiment, the transmission and reception can occur at the same or at different frequencies. When different frequencies are use, one may transmit at a given frequency and create a population distribution for one type of nuclear spin, and upon a magnetization transfer to another type of nucleus, one can detect the signal at a different frequency. Examples of magnetization transfer may include cross-polarization, insensitive nuclei enhanced by polarization transfer (INEPT), distortionless enhancement by polarization transfer (DEPT) or other methods.

[0070] Figs. 10A-C illustrate one embodiment of an MRI setup: Fig. 10A illustrates the rf coil or resonator covers the full sample volume, and surface layers of the conducting region are probed by the pulse sequence. In addition morphological details are probed above the surface via the susceptibility differences between the materials. Fig. 10B illustrates the coil or resonator can be situated above the surface and scan the surface of the material in a setup similar to atomic force microscopy or magnetic resonance force microscopy. The local surface layers are probed by the pulse sequences described. Fig. 10C illustrates morphological details are obtained by (a) probing the surface penetration of the electromagnetic fields and using the pulse sequences (b) probing morphology is also performed by visualizing the changes above the surface.

[0071] In another embodiment, an apparatus is described containing a device for irradiating a sample with a first frequency. In one implementation, in the case of magnetic resonance, this device would be a radio-frequency or microwave coil or resonator/cavity, plus associated amplifiers and pulse controllers. A second device is described for receiving a signal or signals from the sample with a second frequency. The frequencies could be the same, substantially the same, or different. The second device could be a separate detection device comprising a microwave coil or resonator/cavity or resonator tuned to a different frequency. The second device may be hooked up to a preamplifier and the signal digitized for processing.

[0072] In another embodiment, the apparatus used is a conventional NMR spectrometer. Special coils and/or resonators may enhance the performance. In another embodiment, the apparatus may be a conventional MRI imager. Special coils and/or resonators may enhance the performance.

[0073] In another embodiment, the methods include applying a pulse sequence to a conducting region by indirectly detecting microscopic structures of a magnetic susceptibility different from the surrounding material using a gradient echo Magnetic Resonance Imaging experiment observing the surrounding medium, wherein the susceptibility differences are observed through the induced frequency changes. Figs. 11 A-F illustrates a demonstration of frequency changes around a conducting microstructure region, calculated via finite element methods. The histogram shows the frequency distributions. For example, one such high magnetic susceptibility material is metallic dendrites whose dimensions are typically of the order of 10s of micrometers or less. Susceptibility differences on the order of well below 10^{-6} could be observed in this way. Growth of metallic dendrites is a frequent failure mechanism in Li-ion batteries, and some of its alternatives, hence the ability to measure these effects is of importance in the battery field.

[0074] In another embodiment, the methods are applied to a battery, such as a Li-ion battery. In one particular embodiment, a casing 1200 is designed for imaging batteries, fuel cells, or other electrochemical cells, wherein at least one side of the casing is made of non-conducting material to allow radio-frequency fields to enter for analysis. A schematic of one such casing is depicted in Fig. 13A-C as a non-limiting example. The side casing is made of non-conducting material. The battery comprises: a non-conducting cell housing 1201, a conducting end cap 1202, a conducing spring 1203, a conducting current collector

1204, an anode 1205, a separator 1206, and a cathode 1207. The casing 1200 is made to mimic common battery form factors such that real battery materials and geometries can be tested. In the case of Li-ion battery coin cells, this device, assembled with the casing 1200 can be used for noninvasive battery testing, analysis, and imaging, including the surface microscopy techniques described above, for analyzing electrode surfaces, and imaging the surrounding space via indirect effects on the electrolyte. In addition, these techniques could be used to assess the transport properties and quality of electrolytes and separator materials.

[0075] In another embodiment, the method relates to indirectly detecting the volume and porosity of conducting structures by measuring the space around it with NMR spectroscopy or MRI. The volume and morphology of the structures is inferred by induced magnetic susceptibility shifts, which can be amplified by destructive interference by increasing the waiting time in the pulse sequence so that inhomogeneity shifts can evolve for longer times. Susceptibility imaging can be supplemented by machine learning algorithms, wherein the measured images are compared with rapidly generated models of different morphologies, and machine learning algorithms are employed to train an algorithm to recognize the different morphological features in the structures. The susceptibility weighting can be done specifically in the surroundings of a conducting region or within this region, such as a battery as discussed below.

[0076] Examples of calculations and experiments for susceptibility weighted imaging methods are shown in Figs. 11A-F and Figs. 12A-C. Figs. 11 A-F illustrates a demonstration of frequency changes around a conducting microstructure region, calculated via finite element methods. The histogram shows the frequency distributions. Fig. 12A-C illustrate *In situ* ^{1}H 3D FLASH imaging results from an electrochemical cell charged at 160 μA. Fig. 12A shows 2D slices from four time points, Fig. 12B shows segmented images of the results from Fig. 12A where $\boldsymbol{I_{\text{threshold}} = 0.2 I_{\text{max}}}$, Fig. 12C shows 3D segmented images of the same time points with an additional Gaussian filter applied to smoothen the visualization.

[0077] In another embodiment, the method comprises tuning excitation pulse/repetition time to maximize the contrast afforded by inhomogeneities in the excitation/detection rf field amplitude and phase. The tuning of the excitation pulse/repetition time may be based on estimates from rf field calculations on representative systems or based on the general trends found from such calculations.

[0078] Implementations described in this specification can be implemented in digital electronic circuitry, or in computer software, firmware, or hardware, including the structures disclosed in this specification and their structural equivalents, or in combinations of one or more of them. The implementations described in this specification can be implemented as one or more computer programs, i.e., one or more modules of computer program instructions, encoded on one or more computer storage media for execution by, or to control the operation of, data processing apparatus. Alternatively or in addition, the program instructions can be encoded on an artificially-generated propagated signal, e.g., a machine-generated electrical, optical, or electromagnetic signal that is generated to encode information for transmission to suitable receiver apparatus for execution by a data processing apparatus. A computer storage medium can be, or be included in, a computer-readable storage device, a computer-readable storage substrate, a random or serial access memory array or device, or a combination of one or more of them. Moreover, while a computer storage medium is not a propagated signal, a computer storage medium can be a source or destination of computer program instructions encoded in an artificially-generated propagated signal. The computer storage medium can also be, or be included in, one or more separate components or media (e.g., multiple CDs, disks, or other storage devices). Accordingly, the computer storage medium is both tangible and non-transitory.

[0079] As shown in Fig. 9, e.g., a computer-accessible medium 120 (e.g., as described herein, a storage device such as a hard disk, floppy disk, memory stick, CD-ROM, RAM, ROM, etc., or a collection thereof) can be provided (e.g., in communication with the processing arrangement 110). The computer-accessible medium 120 may be a non-transitory computer-accessible medium. The computer-accessible medium 120 can contain executable instructions 130 thereon. In addition or alternatively, a storage arrangement 140 can be provided separately from the computer-accessible medium 120, which can provide the instructions to the processing arrangement 110 so as to configure the processing arrangement to execute certain exemplary procedures, processes and methods, as described herein, for example. The instructions may include a plurality of sets of instructions. For example, in some implementations, the instructions may include instructions for applying radio frequency energy in a plurality of sequence blocks to a volume, where each of the sequence blocks includes at least a first stage. The instructions may further include instructions for repeating the first stage successively until magnetization at a beginning of each of the sequence blocks is stable, instructions for concatenating a plurality of imaging segments, which correspond to the plurality of sequence blocks, into a single continuous imaging segment, and instructions for encoding at least one relaxation parameter into the single continuous imaging segment.

[0080] System 100 may also include a display or output device, an input device such as a key-board, mouse, touch screen or other input device, and may be connected to additional systems via a logical network. Many of the embodiments described herein may be practiced in a networked environment using logical connections to one or more remote computers having processors. Logical connections may include a local area network (LAN) and a wide area network (WAN) that are presented here by way of example and not limitation. Such networking environments are commonplace in office-wide or enterprise-wide computer networks, intranets and the Internet and may use a wide variety of different communication protocols. Those skilled in the art can appreciate that such network computing environments can typically encompass many types of computer system configurations, including personal computers, hand-held devices, multi-processor systems, microprocessor-based or programmable consumer electronics, network PCs, minicomputers, mainframe computers, and the like. Embodiments of the invention may also be practiced in distributed computing environments where tasks are performed by local and remote processing devices that are linked (either by hardwired links, wireless links, or by a combination of hardwired or wireless links) through a communications network. In a distributed computing environment, program modules may be located in both local and remote memory storage devices.

[0081] Various embodiments are described in the general context of method steps, which may be implemented in one embodiment by a program product including computer-executable instructions, such as program code, executed by computers in networked environments. Generally, program modules include routines, programs, objects, components, data structures, etc. that perform particular tasks or implement particular abstract data types. Computer-executable instructions, associated data structures, and program modules represent examples of program code for executing steps of the methods disclosed herein. The particular sequence of such executable instructions or associated data structures represents examples of corresponding acts for implementing the functions described in such steps.

[0082] Software and web implementations of the present invention could be accomplished with standard programming techniques with rule based logic and other logic to accomplish the various database searching steps, correlation steps, comparison steps and decision steps. It should also be noted that the words "component" and "module," as used herein and in the claims, are intended to encompass implementations using one or more lines of software code, and/or hardware implementations, and/or equipment for receiving manual inputs.

[0083] With respect to the use of substantially any plural and/or singular terms herein, those having skill in the art can translate from the plural to the singular and/or from the singular to the plural as is appropriate to the context and/or application. The various singular/plural permutations may be expressly set forth herein for the sake of clarity. In some cases, the actions recited in the claims can be performed in a different order and still achieve desirable results. In addition, the processes depicted in the accompanying figures do not necessarily require the particular order shown, or sequential order, to achieve desirable results. In certain implementations, multitasking and parallel processing may be advantageous. Thus, particular implementations of the invention have been described.

[0084] The foregoing description of illustrative embodiments has been presented for purposes of illustration and of description. It is not intended to be exhaustive or limiting with respect to the precise form disclosed, and modifications and variations are possible in light of the above teachings or may be acquired from practice of the disclosed embodiments. Therefore, the above embodiments should not be taken as limiting the scope of the invention.

WHAT IS CLAIMED IS

1. A method of probing the layers above, at, and below the surface of a conducting region comprising:

exciting nuclear or electronic spins within the conducting region using a first

frequency; and

receiving a second frequency from the conducting region;

determining the length scales by the conductivity of the conducting region, the

first frequency, and the second frequency;

obtaining a depth profile of the conducting region;

indirectly measure the presence of the surface by characterizing signal distortions above the surface.

2. The method of probing the layers above, at, and below the surface of a conducting region of claim 1 wherein the conducting region is selected from a group consisting of a metallic conductor, a semi-conductor, a plasma, an electrolyte solution, and a superconductor.

3. The method of probing the layers above, at, and below the surface of a conducting region of claim 1 further comprising tuning the length scale by choosing the operating frequencies.

4. The method of probing the layers above, at, and below the surface of a conducting region of claim 1 wherein the first frequency is the same as the second frequency

5. The method of probing the layers above, at, and below the surface of a conducting region of claim 1 wherein the first frequency is different from the second frequency.

6. The method of probing the layers above, at, and below the surface of a conducting region of claim 5 where the difference in the first frequency and the second frequency are different due to magnetization transfer, the magnetization transfer being due to selection from a group consisting of cross-polarization, INEPT, and DEPT.

7. The method of probing the layers above, at, and below the surface of a conducting region of claim 1 wherein the receiving step is done using the induced magnetic flux in a detection coil by the precessing spin magnetization.

8. The method of probing the layers above, at, and below the surface of a conducting region of claim 7 further comprising applying a shape function to the signal received from the detection coil, wherein the shape function directly scales the detected signal at each depth.

9. The method of probing the layers above, at, and below the surface of a conducting region of claim 1 further comprising the first frequency flipping a plurality of nuclear or electron spins in the conducting region.

10. The method of probing the layers above, at, and below the surface of a conducting region of claim 9 further comprising detecting the precession motion of the plurality of nuclear or electron spins that have been flipped by the first frequency.

11. A method of applying a pulse sequence to a region containing a conducting region comprising:

applying a pulse sequence comprising several rf pulses and delays,

impregnating the conducting region with a certain pattern of z-magnetization; and

reading out the pattern of the z-magnetization.

12. The method of applying a pulse sequence to a conducting region of claim 11 wherein the pattern is a result of the application of repeated pulses which are attenuated and phase-shifted within the conducting region.

13. The method of applying a pulse sequence to a conducting region of claim 11 further comprising adjusting the z-magnetization pattern within the conducting region by a technique selected from 1) altering delays, pulse flip angles and repeats in the pulse sequence, 2) by the repeat of the pulse sequence with modified rf pulse phases, 3) by induced changes in conductivity within the layers, and 4) by changes in magnetic resonance relaxation parameters.

14. The method of applying a pulse sequence to a conducting region of claim 11 wherein the selected technique is by the repeat of the pulse sequence with modified rf pulse phases and wherein the adjusting the z-magnetization pattern results in the reduction of the presence of signals from different slice regions.

15. The method of applying a pulse sequence to a conducting region of claim 11 further comprising using repeating measurements obtained from the reading out the pattern step to quantify the concentration of electron or nuclear spins within the conducting region.

16. The method of applying a pulse sequence to a conducting region of claim 11 further comprising using the read out pattern of z-magnetization to measure one of magnetic resonance parameters, diffusion within the conducting region, or flow within the conducting region .

17. The method of applying a pulse sequence to a conducting region of claim 16 wherein the measured diffusion within the conducting region and a depth profile is used in spectroscopy.

18. A method of applying a pulse sequence to a non-conducting region of claim 11, comprising indirectly detecting microscopic structures of high magnetic susceptibility material using a gradient echo Magnetic Resonance Imaging experiment observing the surrounding medium, wherein the induced amplitude and/or phase changes of the detected signal are observed in order to inform on the properties and/or morphology of the microscopic structures.

19. The method of applying a pulse sequence to a non-conducting region of claim 18 further comprising tuning excitation pulse/repetition time to maximize the

contrast afforded by inhomogeneities in the excitation/detection rf field amplitude and phase.

20. A computer-implemented machine for of probing the layers above, at, and below the surface of a conducting region, comprising:

a processor; and

a tangible computer-readable medium operatively connected to the processor and including computer code configured to:

exciting nuclear or electronic spins within the conducting region using a first frequency; and

receiving a second frequency from the conducting region;

determining the length scales by the conductivity of the conducting region, the first frequency, and the second frequency;

obtaining a depth profile of the conducting region;

indirectly measure the presence of the surface by characterizing signal distortions above the surface.

21. A method for indirectly detecting the volume and porosity of conducting structures comprising:

measuring the space around the structure with magnetic resonance;

inferring the volume and porosity of the conducting structure based upon induced magnetic susceptibility shifts.

22. The method of claim 21, further comprising amplifying the induced magnetic susceptibility shifts by destructive interference.

23. A method of imaging a battery comprising:

providing a casing having a least a portion comprising non-conducting material configured to allow radio frequency waves to pass through the portion;

exciting nuclear or electronic spins within a conducting region of the battery using a first

frequency; and

receiving a second frequency from the conducting region;

determining the length scales by the conductivity of the conducting region, the

first frequency, and the second frequency;

obtaining a depth profile of the conducting region; and

indirectly measure the presence of the surface by characterizing signal distortions above the surface.

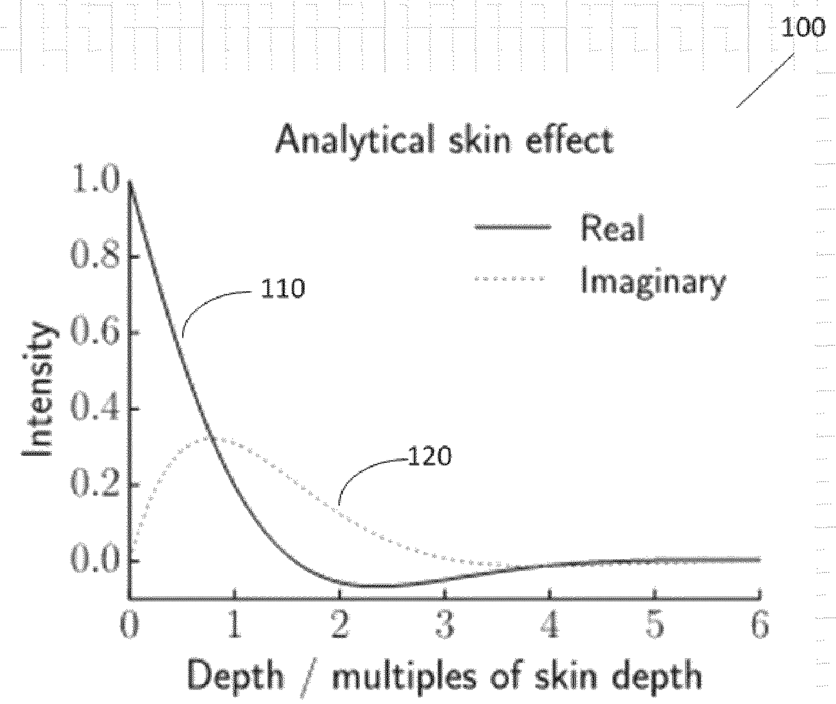
100
Analytical skin effect
Real
Imaginary
110
120
Intensity
1.0
0.8
0.6
0.4
0.2
0.0
0
1
2
3
4
5
6
Depth / multiples of skin depth

Fig. 1

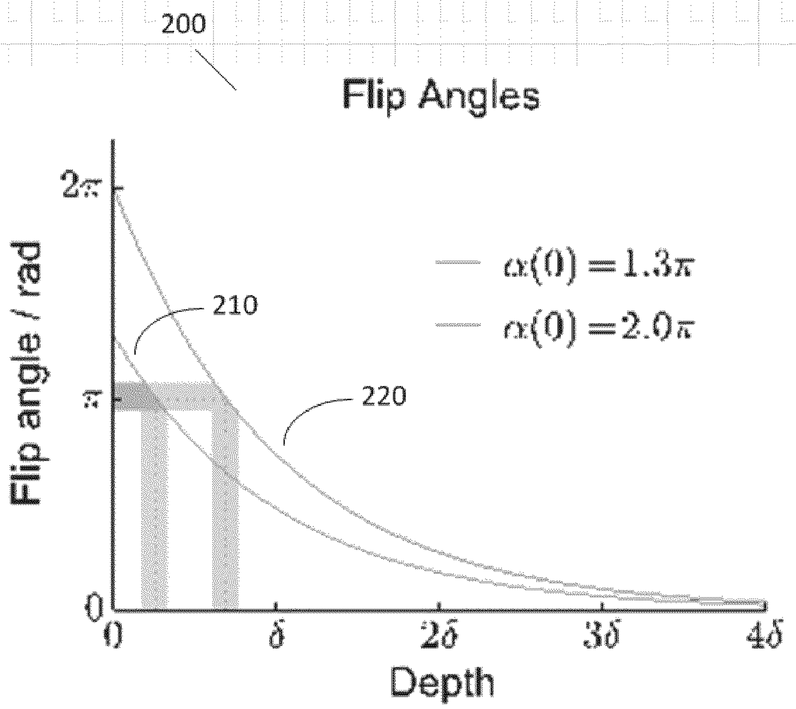
200
Flip Angles
$\alpha(0) = 1.3\pi$
$\alpha(0) = 2.0\pi$
210
220
Flip angle / rad
2π
π
0
0
δ
2δ
3δ
4δ
Depth

Fig. 2

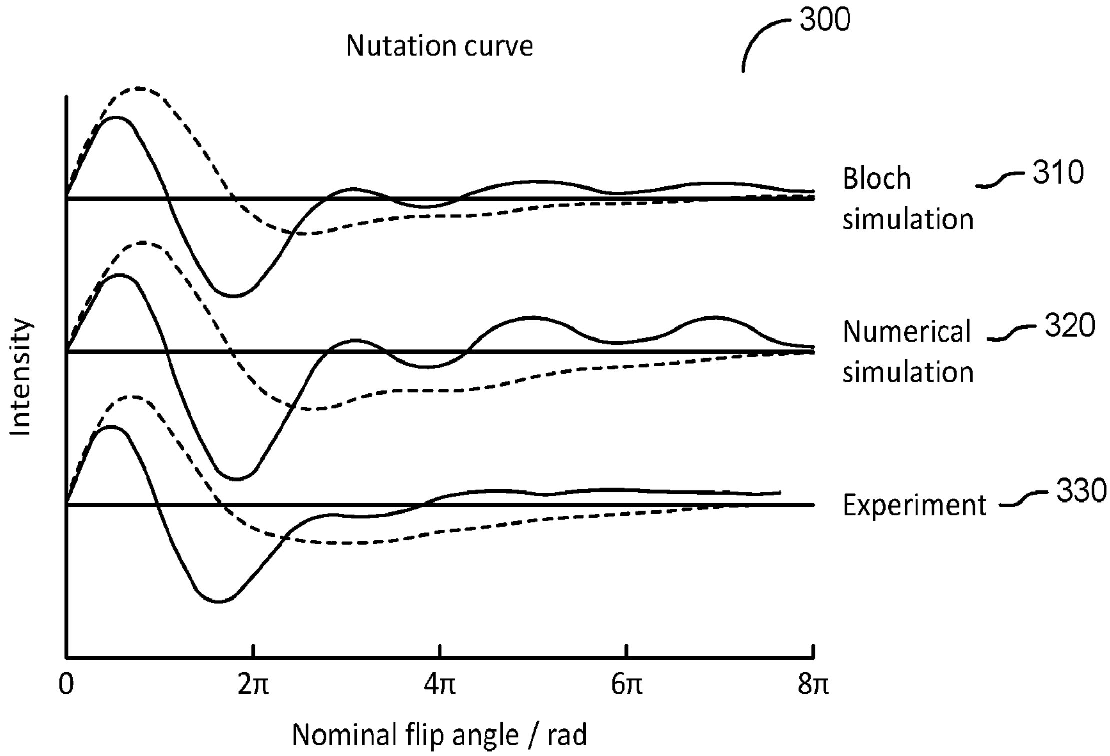
300
Nutation curve
Intensity
Bloch simulation
310
Numerical simulation
320
Experiment
330
0
2π
4π
6π
8π
Nominal flip angle / rad

Fig. 3

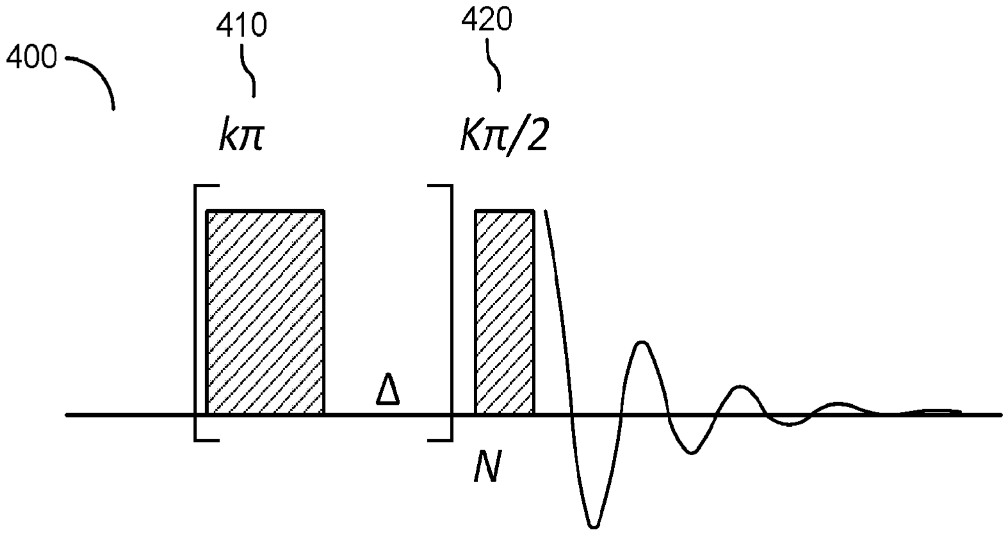
400
410
420
kπ
Kπ/2
Δ
N

Fig. 4

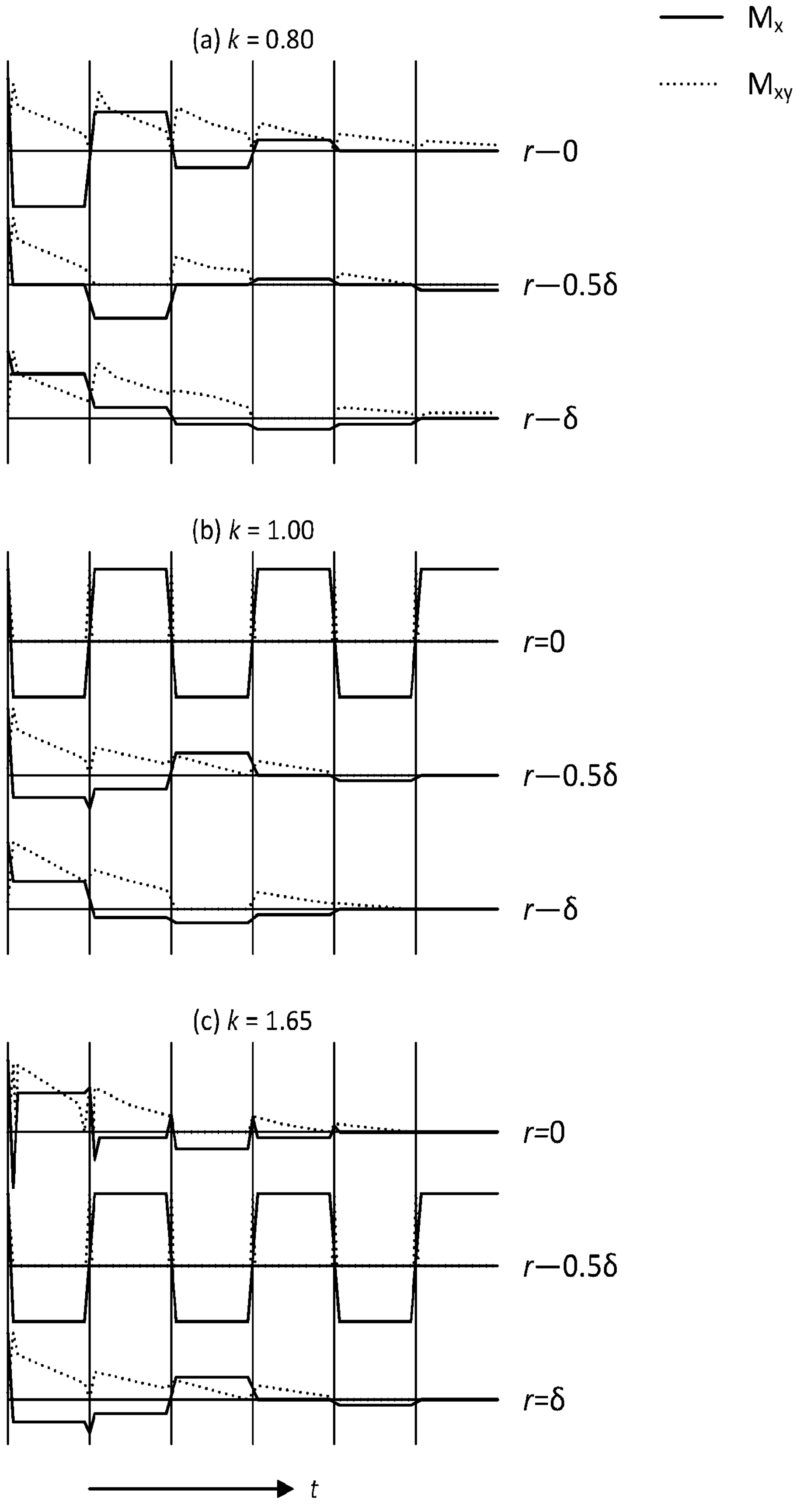

Fig. 5

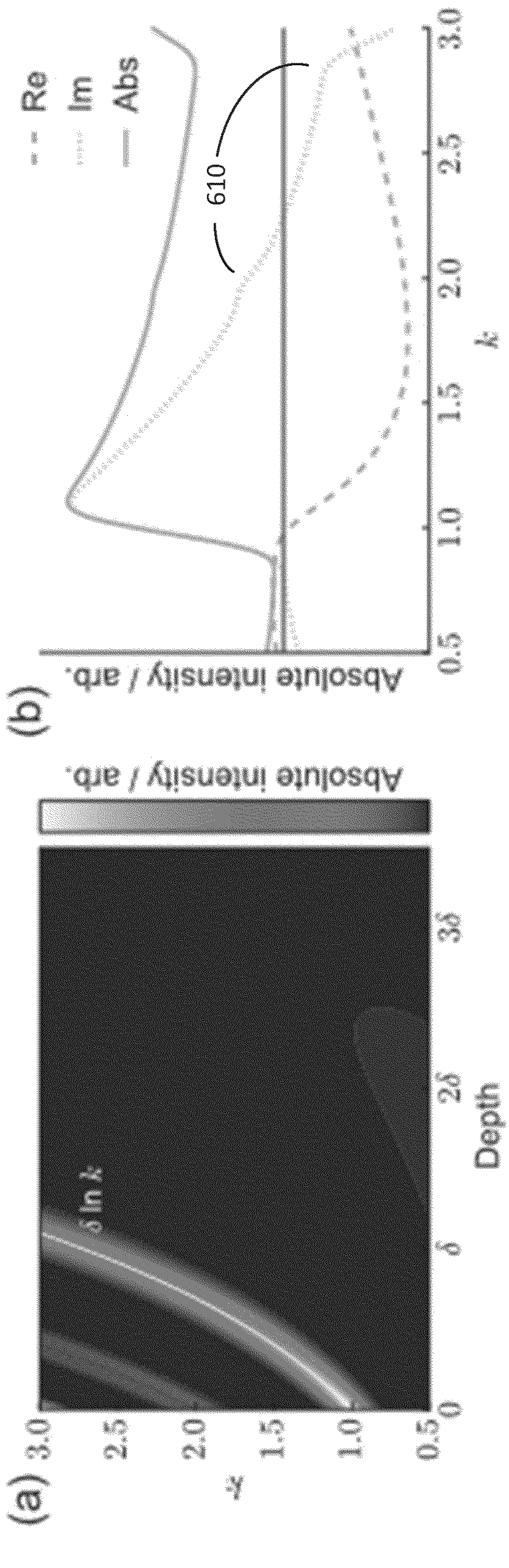
(a)
k
Depth
δ ln k
Absolute intensity / arb.
(b)
Re
Im
Abs
610
k
Absolute intensity / arb.

Fig. 6

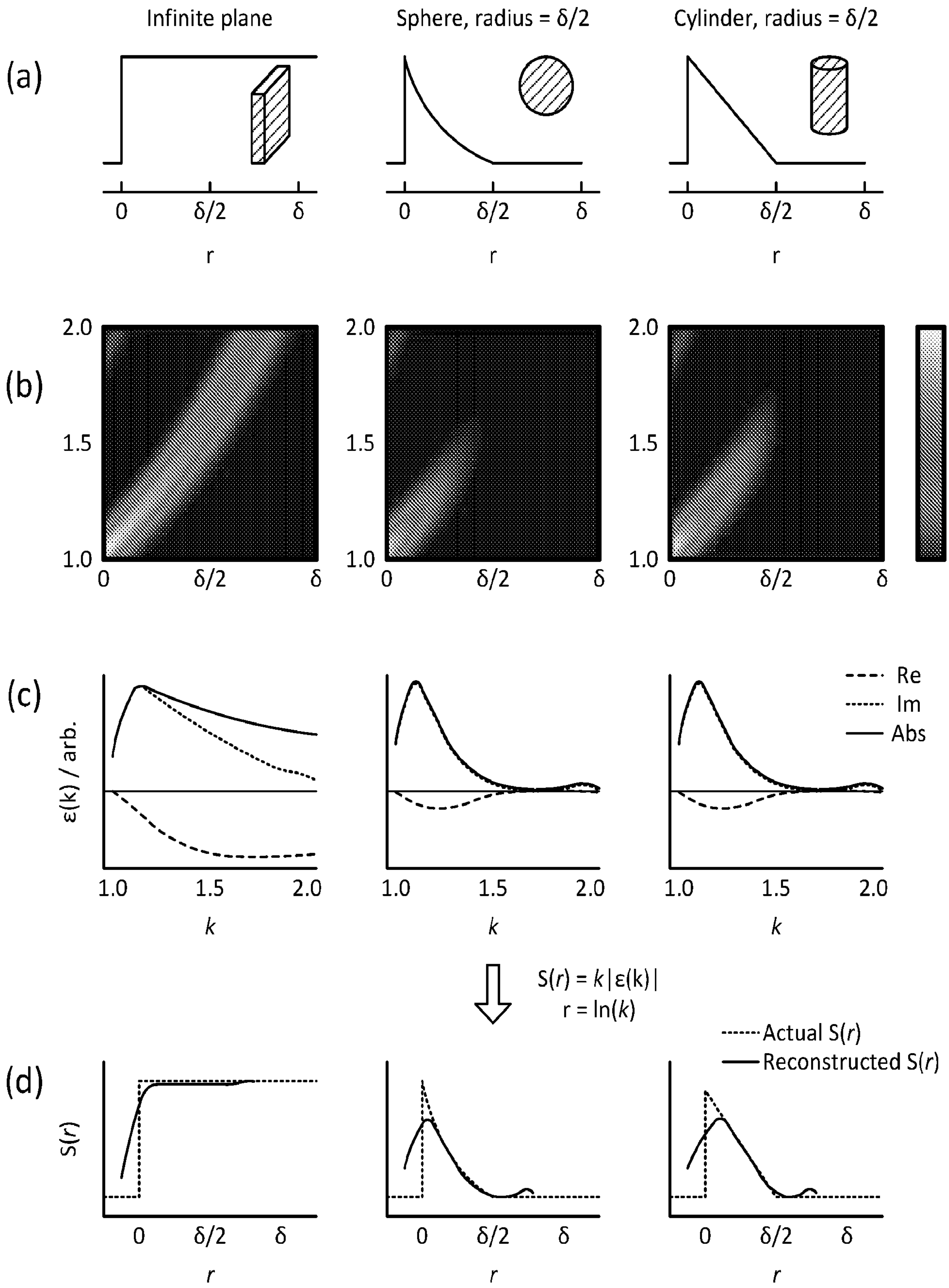
Infinite plane
Sphere, radius = δ/2
Cylinder, radius = δ/2
(a)
0
δ/2
δ
r
(b)
2.0
1.5
1.0
(c)
ε(k) / arb.
Re
Im
Abs
1.0
1.5
2.0
k
S(r) = k|ε(k)|
r = ln(k)
Actual S(r)
Reconstructed S(r)
(d)
S(r)

Fig. 7

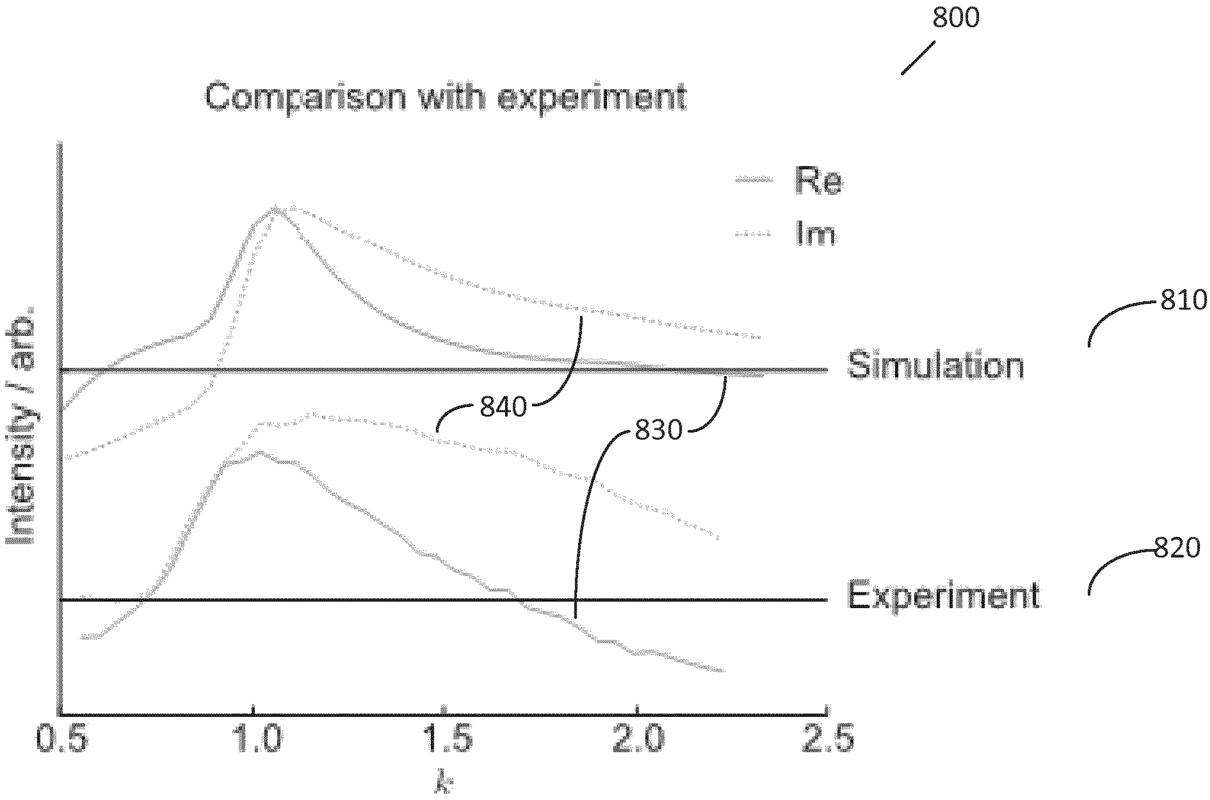
800
Comparison with experiment
Re
Im
810
Simulation
840
830
820
Experiment
Intensity / arb.
0.5
1.0
1.5
2.0
2.5
k

Fig. 8

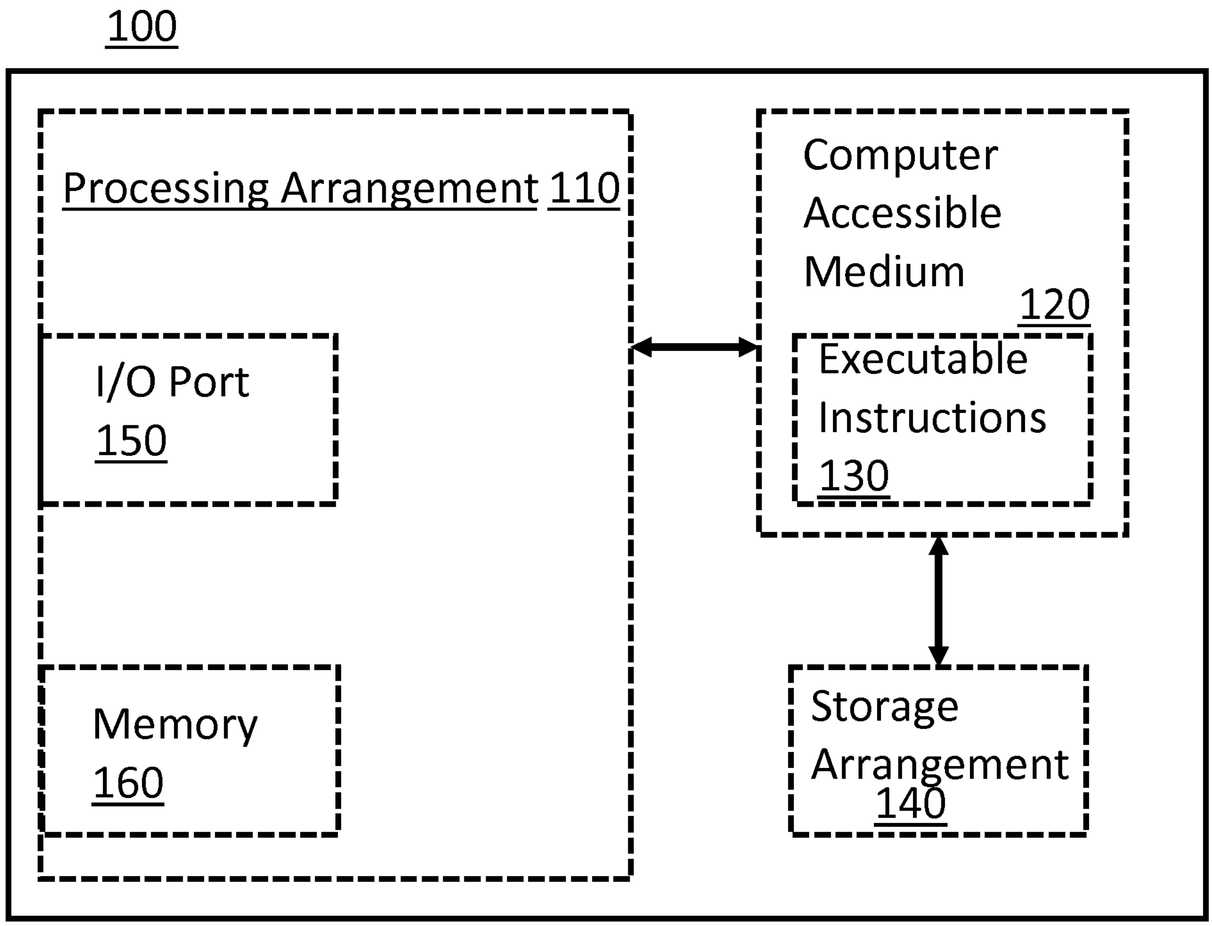
100
Processing Arrangement 110
I/O Port
150
Memory
160
Computer
Accessible
Medium
120
Executable
Instructions
130
Storage
Arrangement
140

Fig. 9

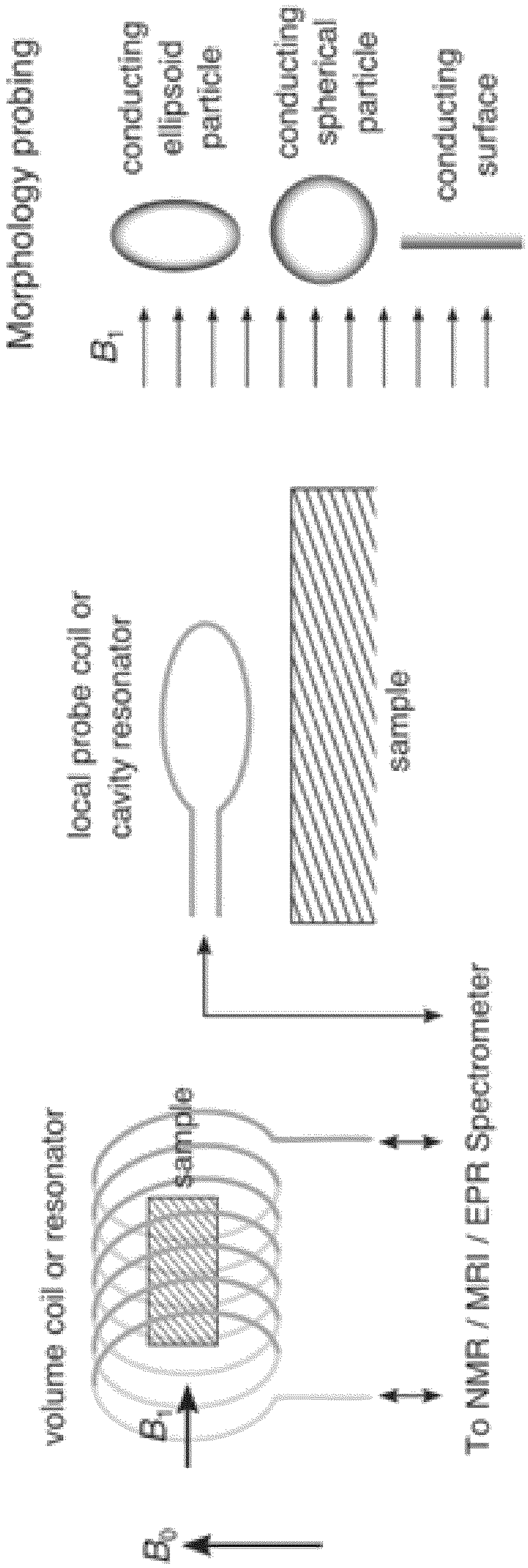

Fig. 10A

Fig. 10B

Fig. 10C

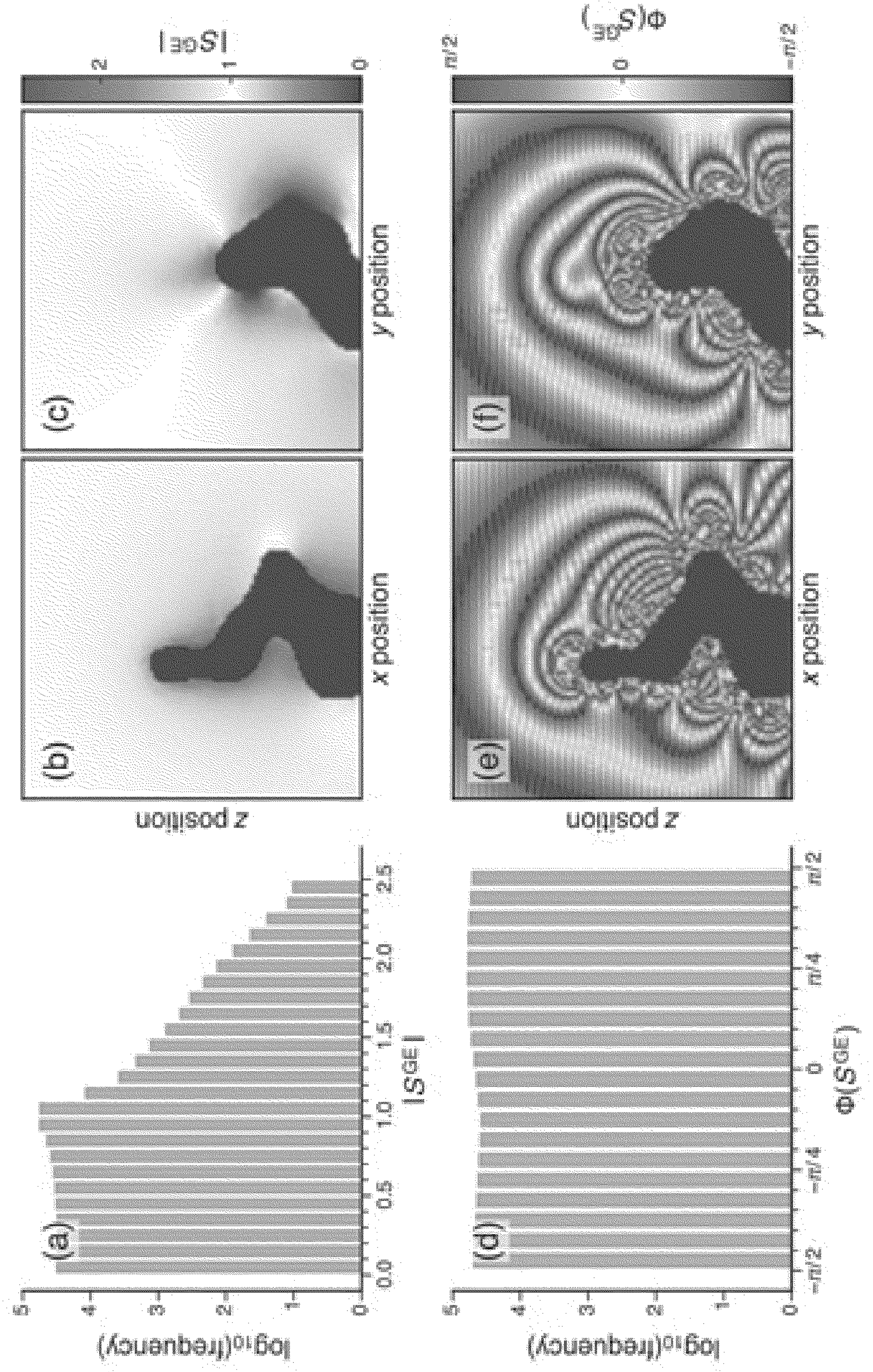

Figs. 11A

Figs. 11B

Figs. 11C

Figs. 11D

Figs. 11E

Figs. 11F

Figs. 12A

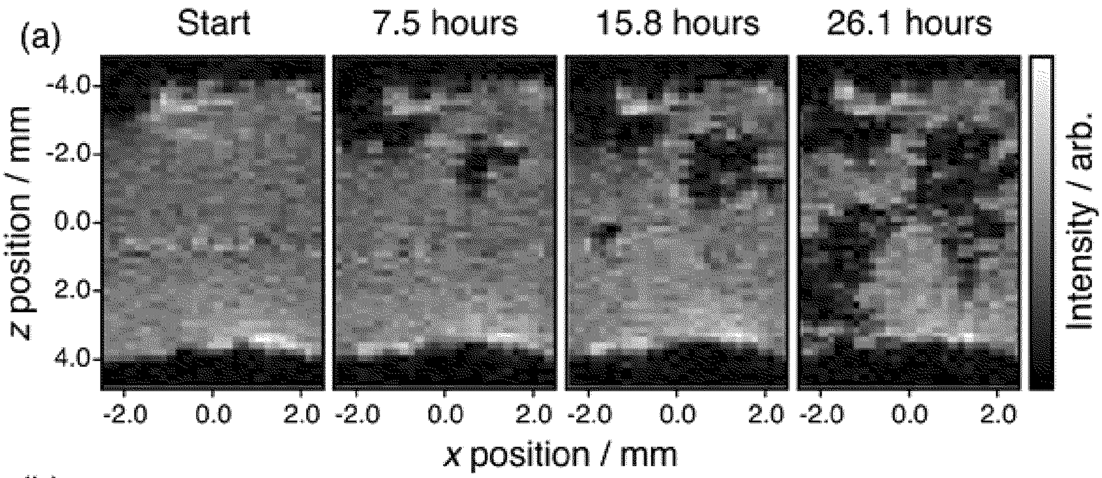

Figs. 12B

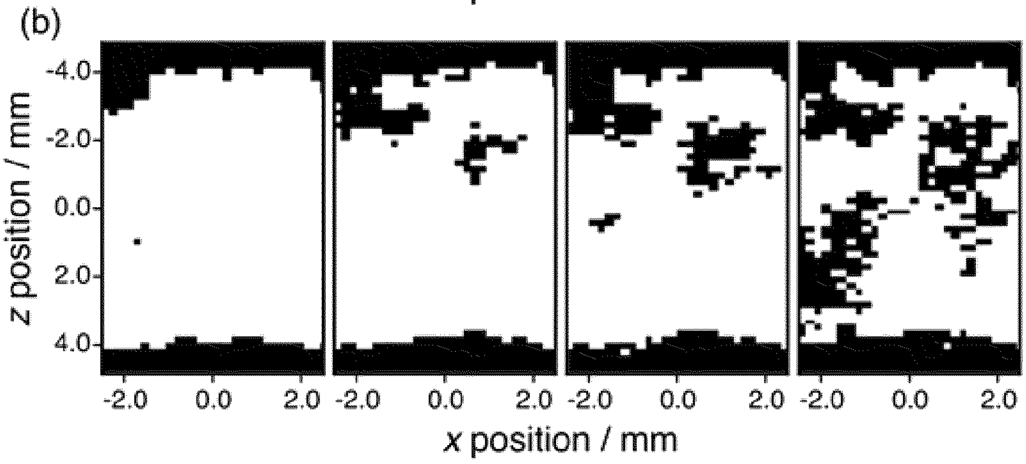

Figs. 12C

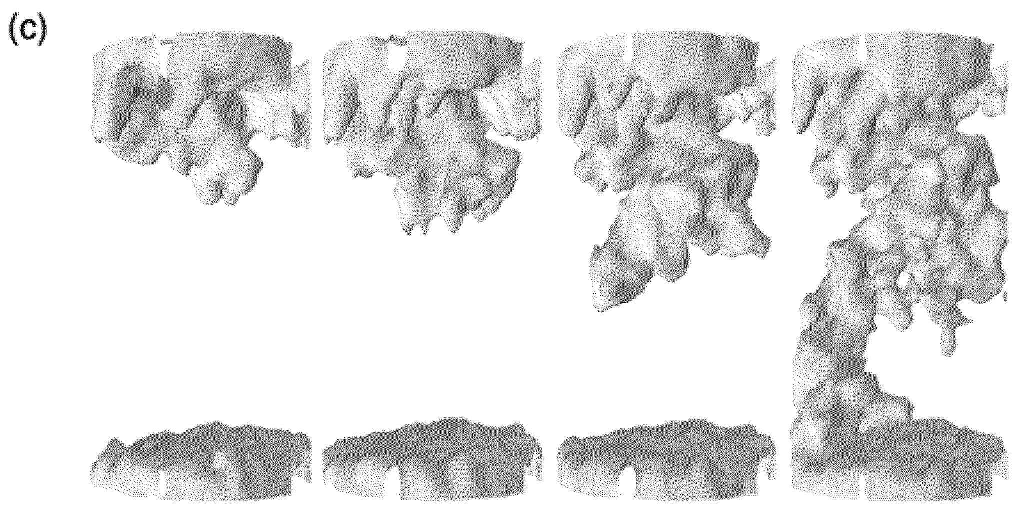

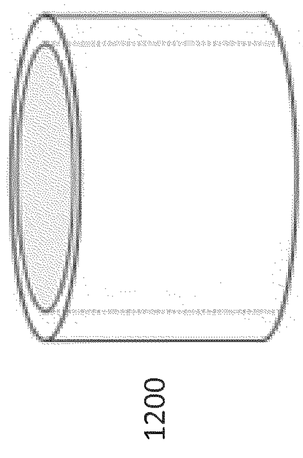

Figure 13A

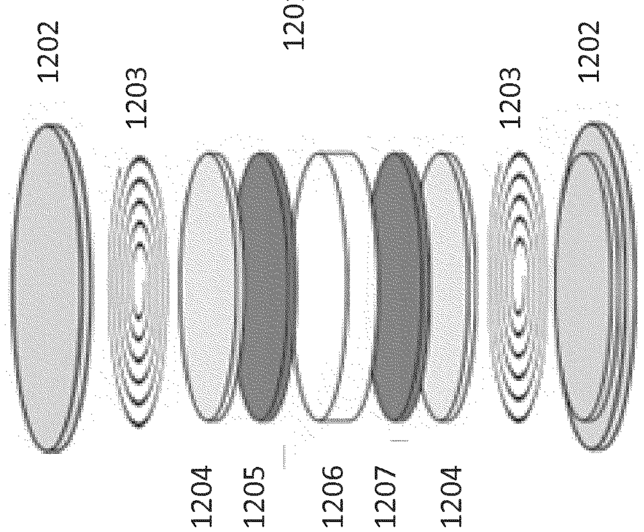

Figure 13B

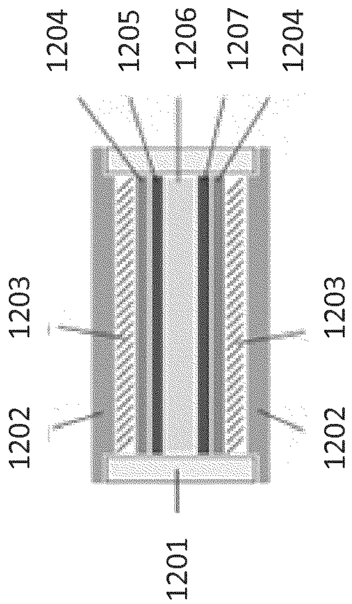

Figure 13C

INTERNATIONAL SEARCH REPORT

International application No.
PCT/US2016/027624

A. CLASSIFICATION OF SUBJECT MATTER

IPC(8) - G01B 7/26; G01B 7/02; G01B 7/28; G01R 33/12; G01R 33/32; G01R 33/422; G06F 1/00 (2016.01)
CPC - G01B 7/26; G01B 7/02; G01B 7/28; G01R 33/1284; G01R 33/32; G01R 33/422 (2016.05)
According to International Patent Classification (IPC) or to both national classification and IPC

B. FIELDS SEARCHED

Minimum documentation searched (classification system followed by classification symbols)
IPC - G01B 7/02; G01B 7/26; G01B 7/28; G01R 33/12; G01R 33/32; G01R 33/422; G06F 1/00; G06F 1/20; G06F 7/00
CPC - G01B 7/02; G01B 7/26; G01B 7/28; G01R 33/1284; G01R 33/32; G01R 33/422; G06T 1/00; G06T 1/0007; G06T 1/20; G06T 7/0022; G06T 7/0051

Documentation searched other than minimum documentation to the extent that such documents are included in the fields searched
USPC - 320/134; 320/136; 324/307; 324/310; 324/311; 324/312; 324/313; 324/316; 702/155; 702/166; 702/167; 702/170 (keyword delimited)

Electronic data base consulted during the international search (name of data base and, where practicable, search terms used)
Orbit, Google Patents, Google Scholar
Search terms used: battery, image, conductive, depth, spin, frequency, scales, length, signal distortion, tune, shape, magnetization transfer, funcation

C. DOCUMENTS CONSIDERED TO BE RELEVANT

Category*	Citation of document, with indication, where appropriate, of the relevant passages	Relevant to claim No.
Y	US 2007/0299628 A1 (SUN) 27 December 2007 (27.12.2007) entire document	1-10, 20, 23
Y	US 2006/0071662 A1 (XIANG et al) 06 April 2006 (06.04.2006) entire document	1-10, 20, 23
Y	US 2008/0231281 A1 (FAIN et al) 25 September 2008 (25.09.2008) entire document	6
Y	US 6,256,603 B1 (CELNIKER) 03 July 2001 (03.07.2001) entire document	8
Y	US 2013/0088204 A1 (VILLANOVA UNIVERSITY) 11 April 2013 (11.04.2013) entire document	23
A	US 2006/0291364 A1 (KOZICKI) 28 December 2006 (28.12.2006) entire document	1-10, 20, 23

☐ Further documents are listed in the continuation of Box C. ☐ See patent family annex.

* Special categories of cited documents:
"A" document defining the general state of the art which is not considered to be of particular relevance
"E" earlier application or patent but published on or after the international filing date
"L" document which may throw doubts on priority claim(s) or which is cited to establish the publication date of another citation or other special reason (as specified)
"O" document referring to an oral disclosure, use, exhibition or other means
"P" document published prior to the international filing date but later than the priority date claimed
"T" later document published after the international filing date or priority date and not in conflict with the application but cited to understand the principle or theory underlying the invention
"X" document of particular relevance; the claimed invention cannot be considered novel or cannot be considered to involve an inventive step when the document is taken alone
"Y" document of particular relevance; the claimed invention cannot be considered to involve an inventive step when the document is combined with one or more other such documents, such combination being obvious to a person skilled in the art
"&" document member of the same patent family

Date of the actual completion of the international search	Date of mailing of the international search report
01 August 2016	19 AUG 2016

Name and mailing address of the ISA/	Authorized officer
Mail Stop PCT, Attn: ISA/US, Commissioner for Patents P.O. Box 1450, Alexandria, VA 22313-1450 Facsimile No. 571-273-8300	Blaine R. Copenheaver PCT Helpdesk: 571-272-4300 PCT OSP: 571-272-7774

INTERNATIONAL SEARCH REPORT

International application No.
PCT/US2016/027624

Box No. II Observations where certain claims were found unsearchable (Continuation of item 2 of first sheet)

This international search report has not been established in respect of certain claims under Article 17(2)(a) for the following reasons:

1. ☐ Claims Nos.:
because they relate to subject matter not required to be searched by this Authority, namely:

2. ☐ Claims Nos.:
because they relate to parts of the international application that do not comply with the prescribed requirements to such an extent that no meaningful international search can be carried out, specifically:

3. ☐ Claims Nos.:
because they are dependent claims and are not drafted in accordance with the second and third sentences of Rule 6.4(a).

Box No. III Observations where unity of invention is lacking (Continuation of item 3 of first sheet)

This International Searching Authority found multiple inventions in this international application, as follows:
See supplemental page

1. ☐ As all required additional search fees were timely paid by the applicant, this international search report covers all searchable claims.

2. ☐ As all searchable claims could be searched without effort justifying additional fees, this Authority did not invite payment of additional fees.

3. ☐ As only some of the required additional search fees were timely paid by the applicant, this international search report covers only those claims for which fees were paid, specifically claims Nos.:

4. ☒ No required additional search fees were timely paid by the applicant. Consequently, this international search report is restricted to the invention first mentioned in the claims; it is covered by claims Nos.:
1-10, 20, 23

Remark on Protest
☐ The additional search fees were accompanied by the applicant's protest and, where applicable, the payment of a protest fee.
☐ The additional search fees were accompanied by the applicant's protest but the applicable protest fee was not paid within the time limit specified in the invitation.
☐ No protest accompanied the payment of additional search fees.

Continued from Box No. III Observations where unity of invention is lacking

This application contains the following inventions or groups of inventions which are not so linked as to form a single general inventive concept under PCT Rule 13.1. In order for all inventions to be examined, the appropriate additional examination fees must be paid.

Group I, claims 1-10,20,23, drawn to probing the layers above, at, and below the surface of a conducting region.
Group II, claims 11-19, drawn to a method of applying a pulse sequence to a region containing a conducting region.
Group III, claims 21-22, drawn to a method for indirectly detecting the volume and porosity of conducting structures.

The inventions listed as Groups I, II and III do not relate to a single general inventive concept under PCT Rule 13.1 because, under PCT Rule 13.2, they lack the same or corresponding special technical features for the following reasons: the special technical feature of the Group I invention: determining the length scales by the conductivity of the conducting region, the first frequency, and the second frequency; obtaining a depth profile of the conducting region as claimed therein is not present in the invention of Groups II and III. The special technical feature of the Group II invention: applying a pulse sequence comprising several rf pulses and delays, impregnating the conducting region with a certain pattern of z-magnetization; and reading out the pattern of the z-magnetization as claimed therein is not present in the invention of Groups I or III. The special technical feature of the Group III invention: measuring the space around the structure with magnetic resonance; inferring the volume and porosity of the conducting structure based upon induced magnetic susceptibility shifts as claimed therein is not present in the invention of Groups I or II.

Groups I, II and III lack unity of invention because even though the inventions of these groups require the technical feature of probing a conducting region, this technical feature is not a special technical feature as it does not make a contribution over the prior art.

Specifically, US 2006/0291364 A1 (KOZICKI) 28 December 2006 (28.12.2006) teaches probing a conducting region (Paras. 29-30).

Since none of the special technical features of the Group I, II or III inventions are found in more than one of the inventions, unity of invention is lacking.